Science Signaling
AAAS

www.sciencesignaling.org/cgi/content/full/10/485/eaai9062/DC1

Supplementary Materials for

In silico modeling identifies CD45 as a regulator of IL-2 synergy in the NKG2D-mediated activation of immature human NK cells

Sayak Mukherjee, Helle Jensen, William Stewart, David Stewart, William C. Ray, Shih-Yu Chen, Garry P. Nolan, Lewis L. Lanier,* Jayajit Das*

*Corresponding author. Email: lewis.lanier@ucsf.edu (L.L.L.); das.70@osu.edu (J.D.)

Published 27 June 2017, *Sci. Signal.* **10**, eaai9062 (2017)
DOI: 10.1126/scisignal.aai9062

This PDF file includes:

Fig. S11. Test of correlation between CD45 expression and CD107a mobilization to the cell surface of human NK cells from donors #4 to #7.
Fig. S12. Matrix plot showing the changes in average protein abundances in $CD56^{bright}$ and $CD56^{dim}$ NK cells in response to IL-2 treatment.
Table S1. Changes in average protein abundances in $CD56^{bright}$ and $CD56^{dim}$ NK cells in response to IL-2.
Table S2. Mass cytometry antibody panel.

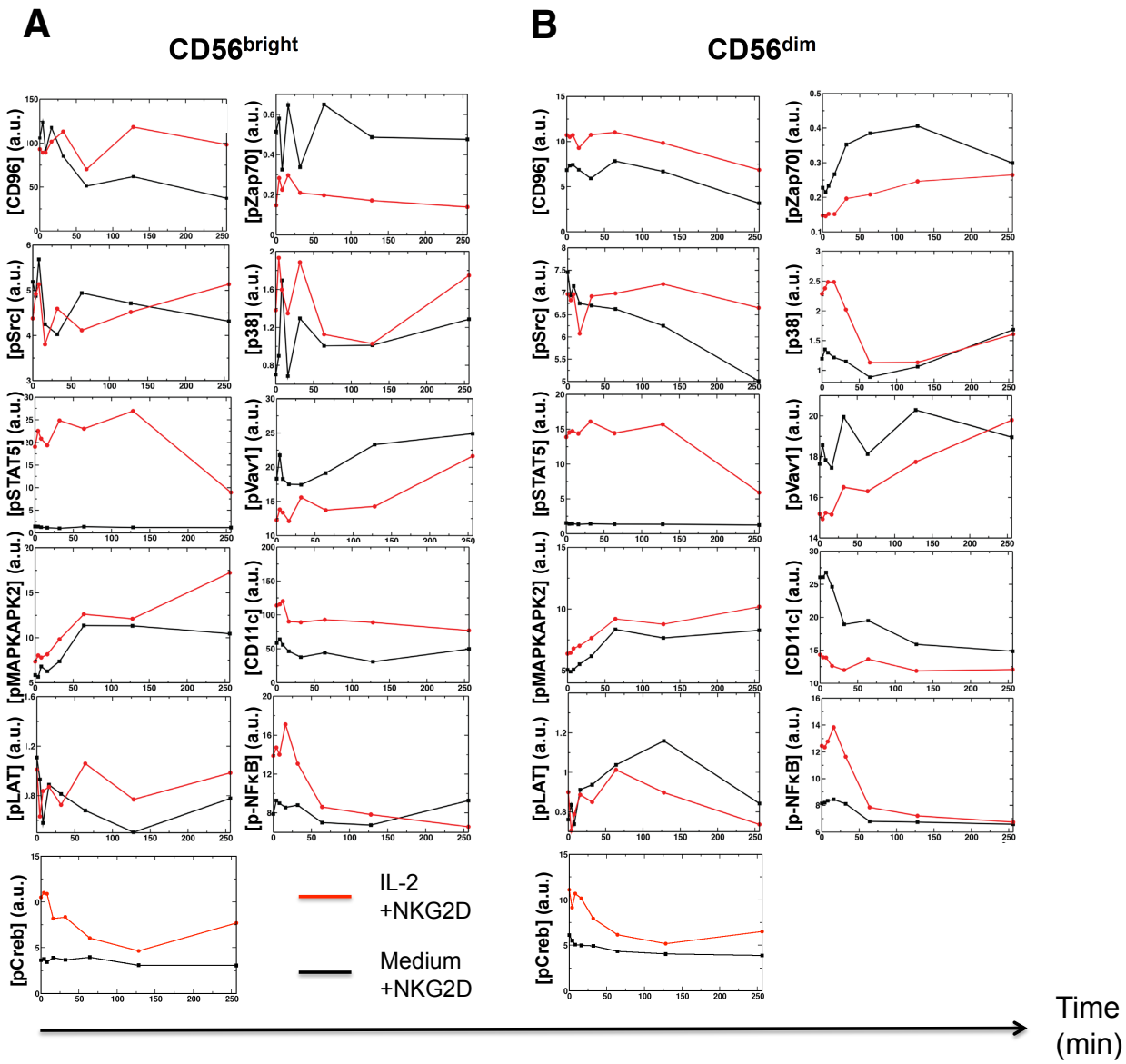

Fig. S1. Kinetics of cell population–averaged protein abundances in mass cytometry measurements in IL-2– or medium-treated CD56^{bright} and CD56^{dim} primary human NK cells (from donor #1) stimulated by anti-NKG2D. (**A** and **B**) Analysis of the kinetics of changes in the average abundances of the indicated proteins in CD56^{bright} (A) and CD56^{dim} (B) primary human NK cells from donor #1. Data are shown at the unstimulated condition (t = 0 min) and at multiple time points (t = 4, 8, 16, 32, 64, 128, and 256 min) after stimulation with anti-NKG2D mAb. Before stimulation through NKG2D, the cells were pre-treated with IL-2 (red trace) or medium (black trace) for 24 hours. Protein abundances were measured by mass cytometry in duplicate samples from each donor. The average protein abundances were calculated from Equation 3a for the cell population in the duplicate samples. The total number of cells (variable N in Equation 3a) was 200 for CD56^{bright} NK cells and 4000 for CD56^{dim} NK cells. a.u., arbitrary units.

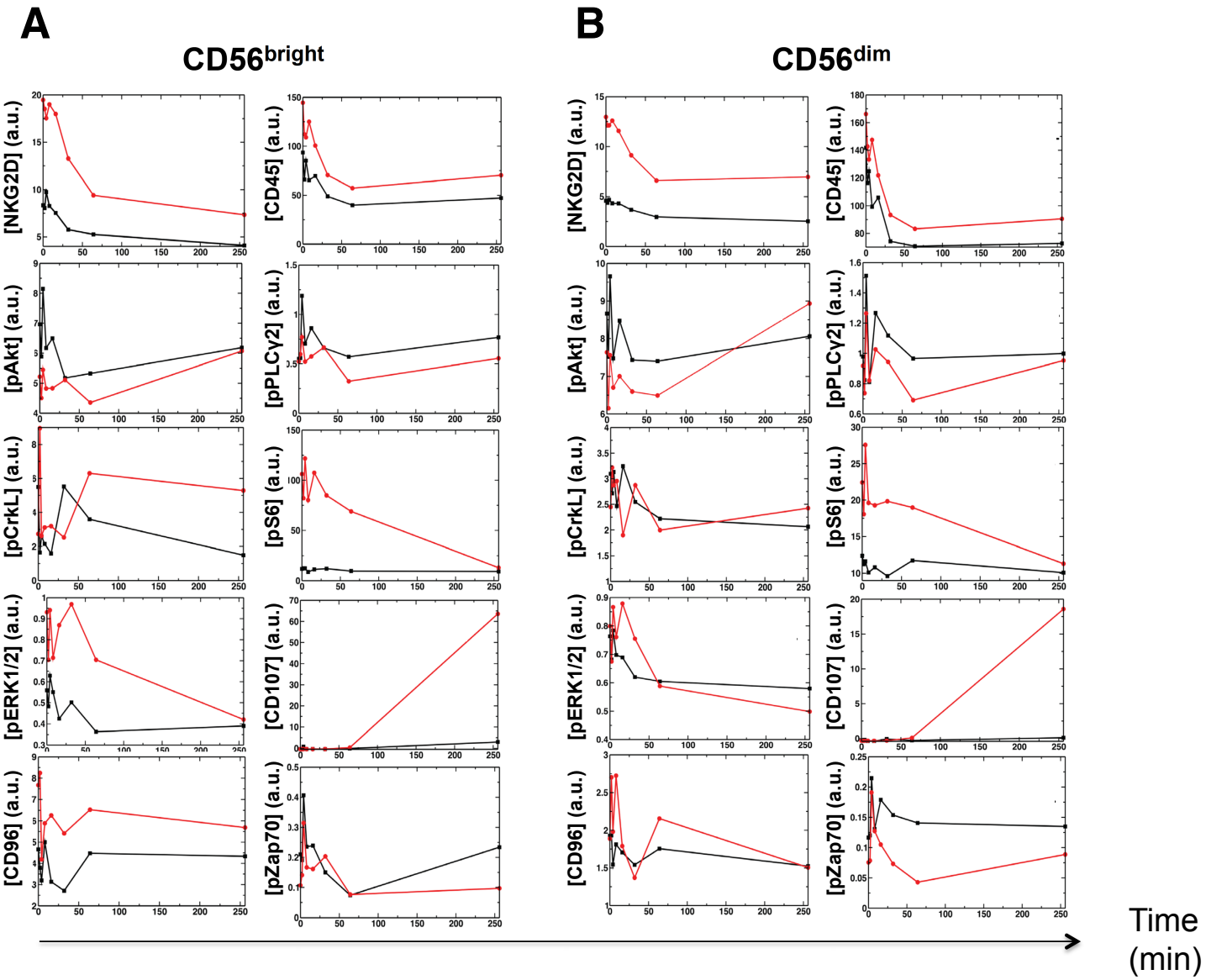
A
CD56bright
B
CD56dim
[NKG2D] (a.u.)
[CD45] (a.u.)
[pAkt] (a.u.)
[pPLCγ2] (a.u.)
[pCrkL] (a.u.)
[pS6] (a.u.)
[pERK1/2] (a.u.)
[CD107] (a.u.)
[CD96] (a.u.)
[pZap70] (a.u.)
Time (min)

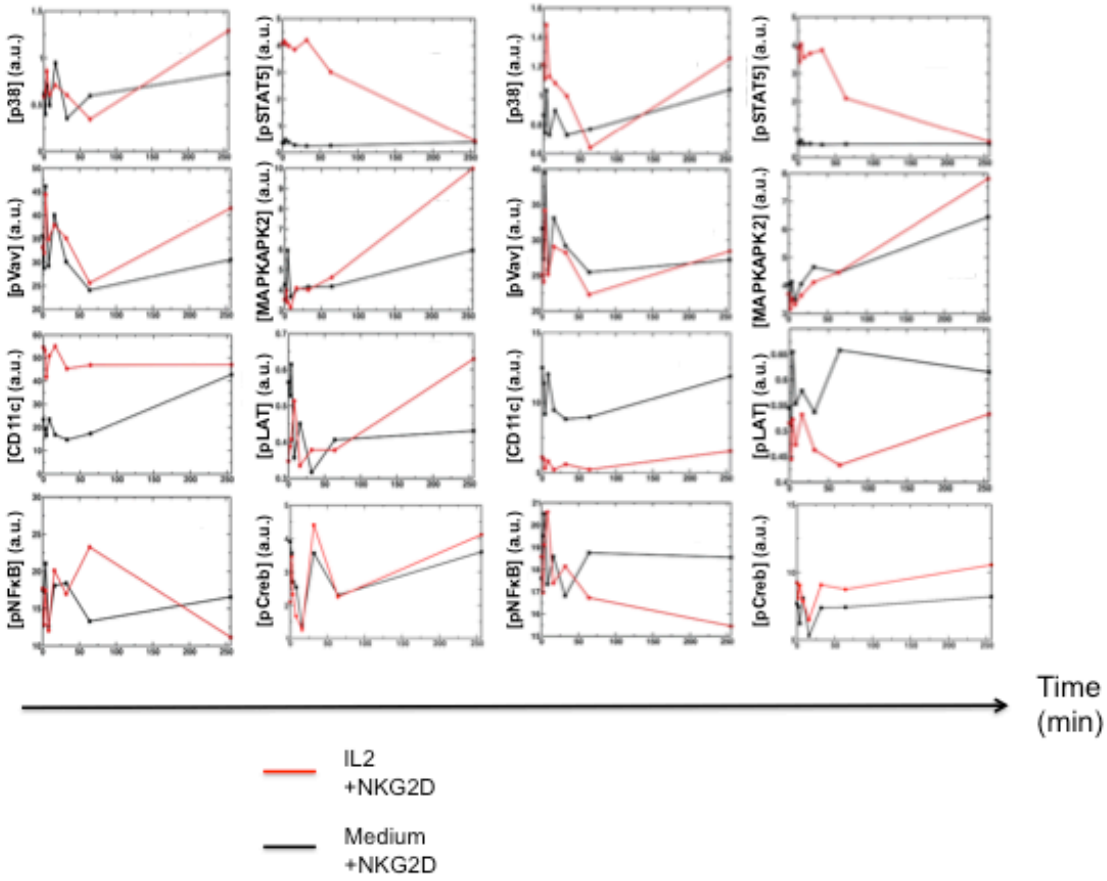

Fig. S2. Kinetics of cell population–averaged protein abundances in mass cytometry measurements in IL-2– or medium-treated CD56^{bright} and CD56^{dim} primary human NK cells (from donor #2) stimulated by anti-NKG2D. (**A** and **B**) Analysis of the kinetics of changes in the average abundances of the indicated proteins in CD56^{bright} (A) and CD56^{dim} (B) primary human NK cells from donor #2. Data are shown at the unstimulated condition (t = 0 min) and at multiple time points (t = 2, 4, 8, 16, 32, 64, and 256 min) after stimulation with anti-NKG2D mAb. Before stimulation through NKG2D, the cells were pretreated with IL-2 (red trace) or medium (black trace) for 24 hours. Protein abundances were measured by mass cytometry in duplicate samples from each donor. The average protein abundances were calculated from Equation 3a for the cell population in the duplicate samples. The total number of cells (variable N in Equation 3a) was 672 for IL-2-pretreated CD56^{bright} NK cells, 1000 for medium-treated CD56^{bright} NK cells, 5300 for IL-2-pretreated CD56^{dim} NK cells, and 10,350 for medium-treated CD56^{dim} NK cells.

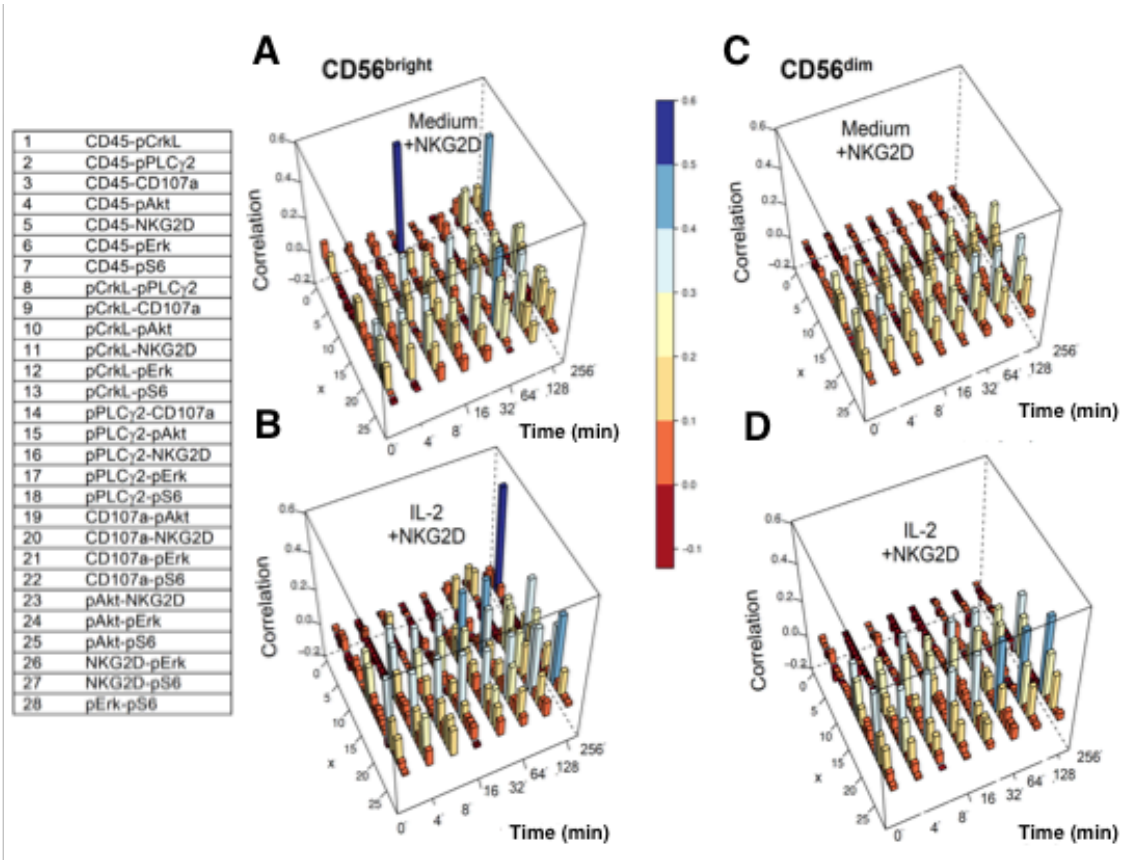

Fig. S3. Kinetics of correlations between protein species in CD56^{bright} and CD56^{dim} NK cells from donor #2. (**A** to **D**) The kinetics of correlations after stimulation with anti-NKG2D mAb for medium- (**A**) or IL-2–treated (**B**) CD56^{bright} NK cells and medium- (**C**) or IL-2–treated (**D**) CD56^{dim} NK cells. The color bars display the colors associated with the magnitudes of correlations. The integers along the axis marked "x" designate the protein pairs for which the correlations were calculated. Each value of the integer corresponds to a specific protein pair shown in the table on the left side of the figure.

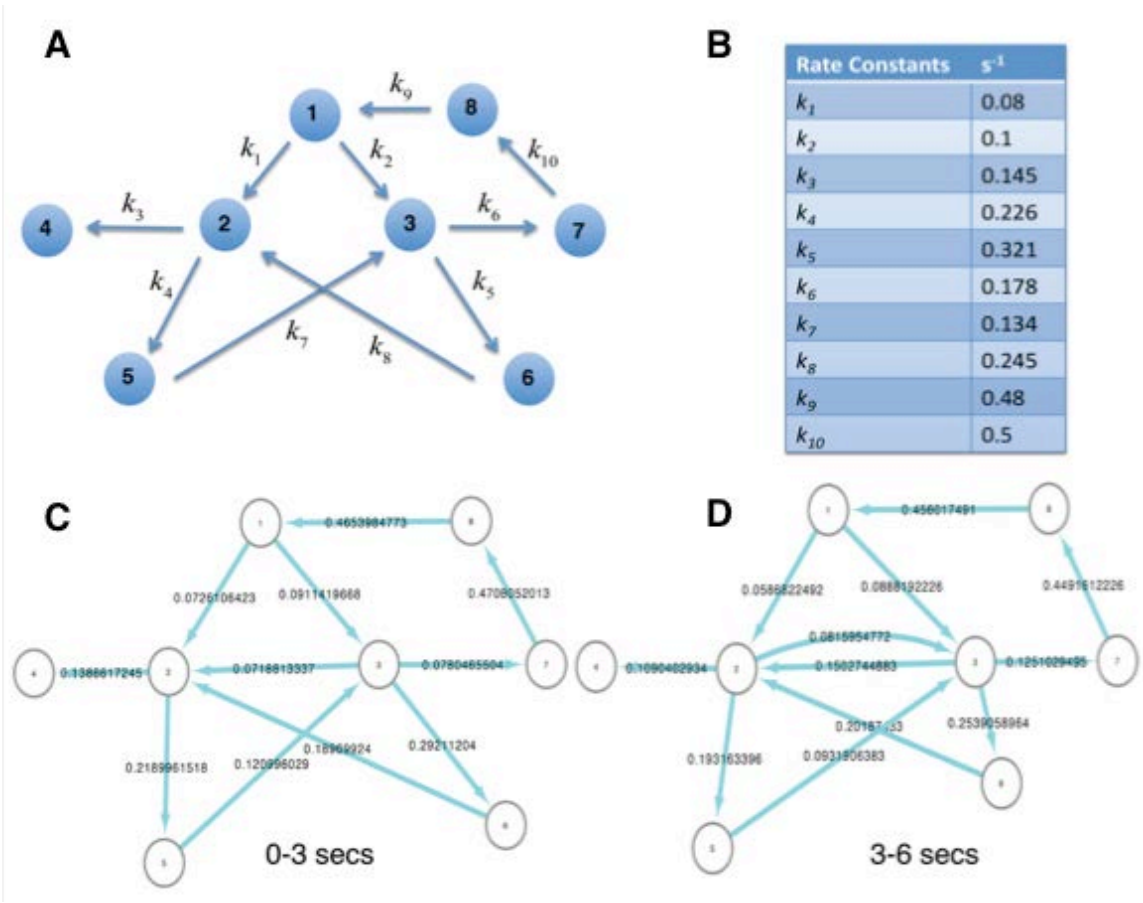

Fig. S4. Estimation of reaction rates with synthetic data generated from a biochemical network composed of coupled first-order chemical reactions. (**A** and **B**) The eight-species linear network that was used to generate the single-cell, time-stamped synthetic data (A). In the model for the linear network, the species abundances follow deterministic, mass-action kinetics described by a set of coupled first-order ordinary differential equations. Each solid blue node represents a distinct protein species. The blue arrows denote the direction of the reaction and should be read as follows: a molecular species 1 transforms itself into another molecular species 2 at a rate k_1. The initial species abundances in single cells were chosen from a multivariate Gaussian distribution. The rate constants are shown in the table in (B). Groups of 3000 cells were used to calculate the average abundances and covariances at different time points. Note that we used a different batch of single cells for each calculation to represent the mass cytometry experiments in which individual cells are destroyed upon a measurement. The calculations were performed at the times, t = 0, 3, 6, and 9 s. (B) The table shows the value of the rate constants used in the simulation of kinetics. (**C**) The rates were estimated with the simulated annealing method described in Materials and Methods and with the time-stamped synthetic data at times $t = 0$ and $t = 3$ s. Unlike the nonlinear Ras-SOS network (fig. S5), the T cell signaling network (fig. S6), and the mass cytometry data (Figs. 4 and 5, and fig. S8), we started the simulated annealing scheme with an initial M matrix in which the off-diagonal elements were chosen at random from a uniform distribution U (0,1). The diagonal elements were chosen in such a way that the sum of the elements in each column of the initial M matrix

was zero. The choice of the initial M matrix for the linear network considered here generated an initial condition that was a more stringent test for the correct estimation of the rate constants. This is because the initial choice does not choose a specific network wiring beforehand (unlike the other examples mentioned earlier); rather, the annealing process takes the system to the correct network wiring. The estimated values are shown on the arrows. Any rate constant below the value of 0.05 s^{-1} was set to 0. The widths of the arrows are proportional to the values of the rate constants. The connection between the nodes 2 and 3 arises as a spurious rate. (**D**) As described for (C), except that time-stamped data at $t = 3$ and $t = 6$ s were used for the estimation. The connections between the nodes 2 and 3 arise as spurious rates.

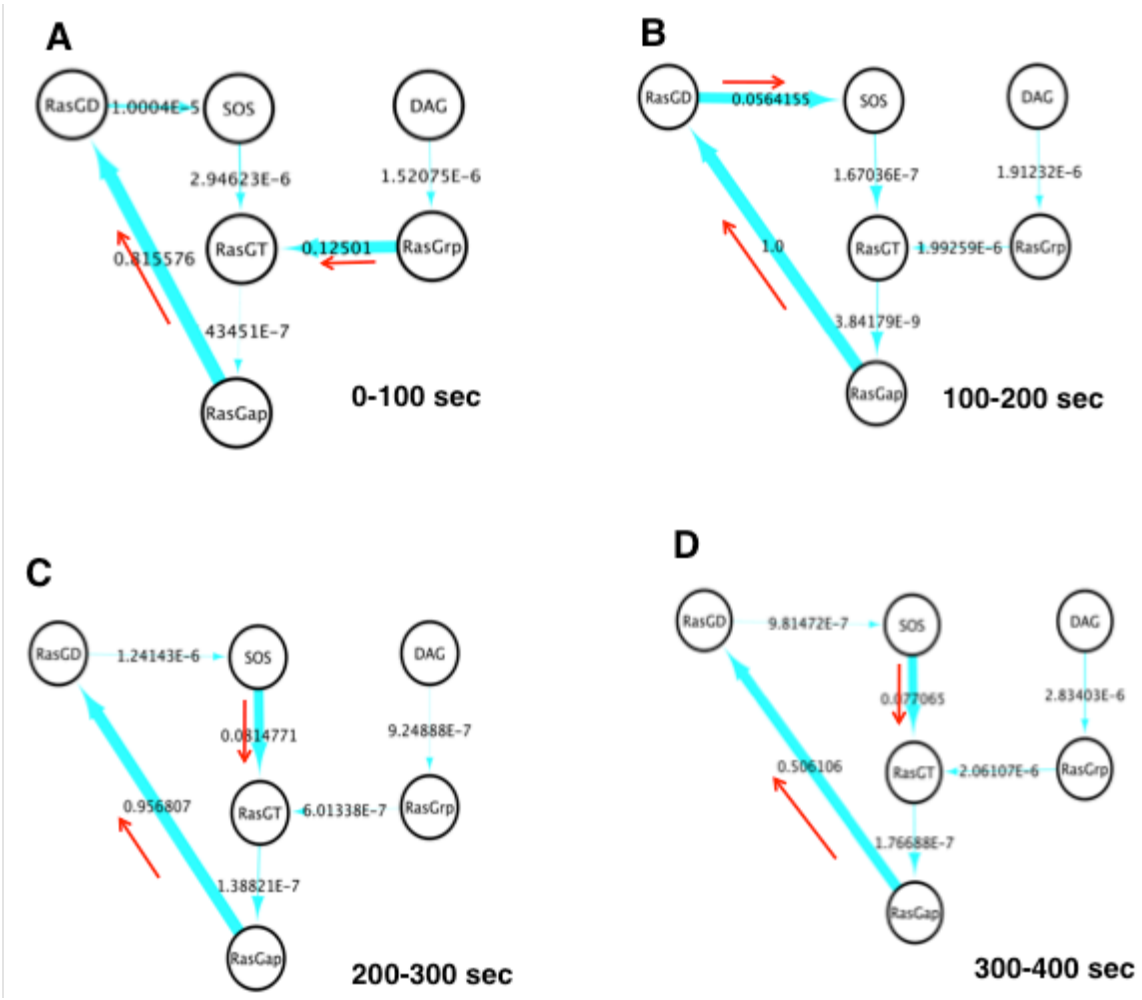
A
RasGD
1.0004E-5
SOS
DAG
2.94623E-6
1.52075E-6
0.815576
RasGT
0.12501
RasGrp
43451E-7
RasGap
0-100 sec
B
RasGD
0.0564155
SOS
DAG
1.67036E-7
1.91232E-6
1.0
RasGT
1.99259E-6
RasGrp
3.84179E-9
RasGap
100-200 sec
C
RasGD
1.24143E-6
SOS
DAG
0.0814771
9.24888E-7
0.956807
RasGT
6.01338E-7
RasGrp
1.38821E-7
RasGap
200-300 sec
D
RasGD
9.81472E-7
SOS
DAG
0.077065
2.83403E-6
0.506106
RasGT
2.06107E-6
RasGrp
1.76688E-7
RasGap
300-400 sec

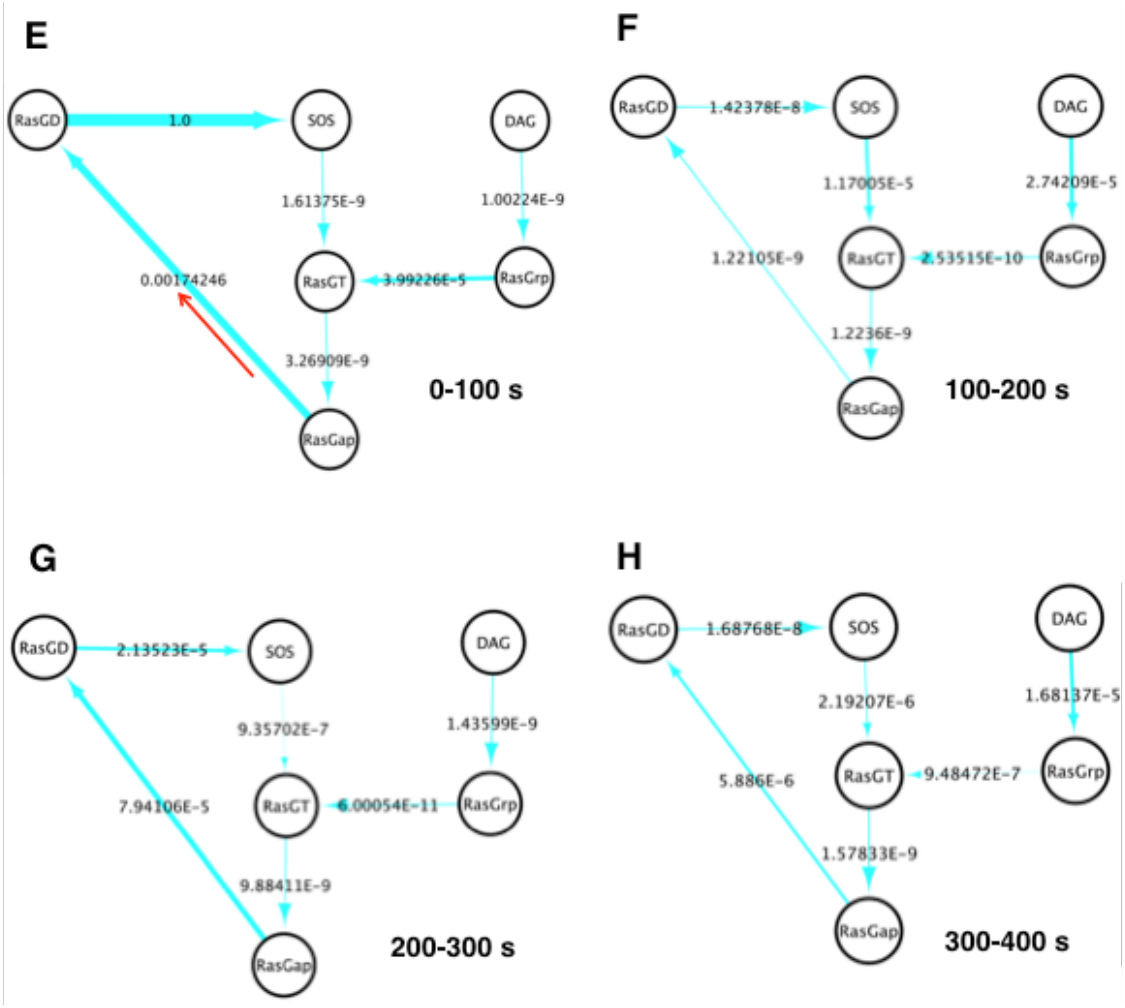

Fig. S5. Estimation of reaction rates with synthetic data generated from the Ras activation network composed of coupled, nonlinear chemical reactions. (**A** to **H**) We investigated signal propagation in the Ras activation network with synthetic, single-cell data generated by simulating a previously published in silico model (*14*). In the Ras activation network, the inactive form of Ras (RasGDP) becomes active (RasGTP) by the action of two RasGEFs, SOS and RasGRP1. Diacylglycerol (DAG), a second messenger generated upon receptor stimulation (for example, of the TCR), binds to RasGRP1 and the complex mediates Ras activation. In addition to the catalytic site in SOS, there is an allosteric site that binds to RasGTP or RasGDP and substantially increases the catalytic rate of SOS. This mediates a positive feedback in Ras activation, which results in bistability in the kinetics. The enzyme RasGAP deactivates Ras (RasGTP→RasGDP). The signaling network has 14 different protein and protein complex species. The biochemical network was simulated by solving the corresponding Master equation with the software package BIONETGEN (bionetgen.org). We provide the BIONETGEN code at the following URL: http://planetx.nationwidechildrens.org/~jayajit/ras_activation. In the synthetic CyTOF measurement, we considered six different species shown in the diagram. The initial species abundances for six protein species, namely (i) SOS, (ii) RasGDP, (iii) RasGTP, (iv) RasGAP, (v) RasGRP1, and (vi) DAG, were drawn from a Gaussian distribution. All other

intermediate complexes were set to zero at the beginning of the simulation. Groups of ten thousand cells were used to calculate averages and correlations. Based on the known signaling pathways between these species, we calculated fluxes for the network shown here. (A to D) Fluxes in the network calculated with the synthetic data during the indicated time intervals. The fluxes were then rescaled by the largest flux so that the relative fluxes shown lie between 0 and 1. As expected, at early times (0 to 100 s), RasGRP1 is mainly involved in Ras activation, whereas RasGAP mediates Ras deactivation. As RasGTP is produced, it binds to the allosteric pocket of SOS, which increases the catalytic rate of SOS. Thus, SOS becomes involved in Ras activation at intermediate and later time points. This captures the known results for Ras activation (*14*). (E to H) We also simulated Ras activation in which the allosteric pocket of SOS is unable to bind to RasGTP or RasGDP. Thus, the system is devoid of any positive feedback and generates very low Ras activation. The calculated fluxes show dominance of Ras deactivation by RasGAP at early times. As expected, RasGRP1 results in little Ras activation (flux ~ 10^{-5}) at early times (0 to 100 s), whereas in the absence of positive feedback, SOS barely contributes to Ras activation (flux ~ 10^{-9}). Thus, our scheme reproduces the correct mechanisms underlying Ras activation, which is a highly nonlinear network.

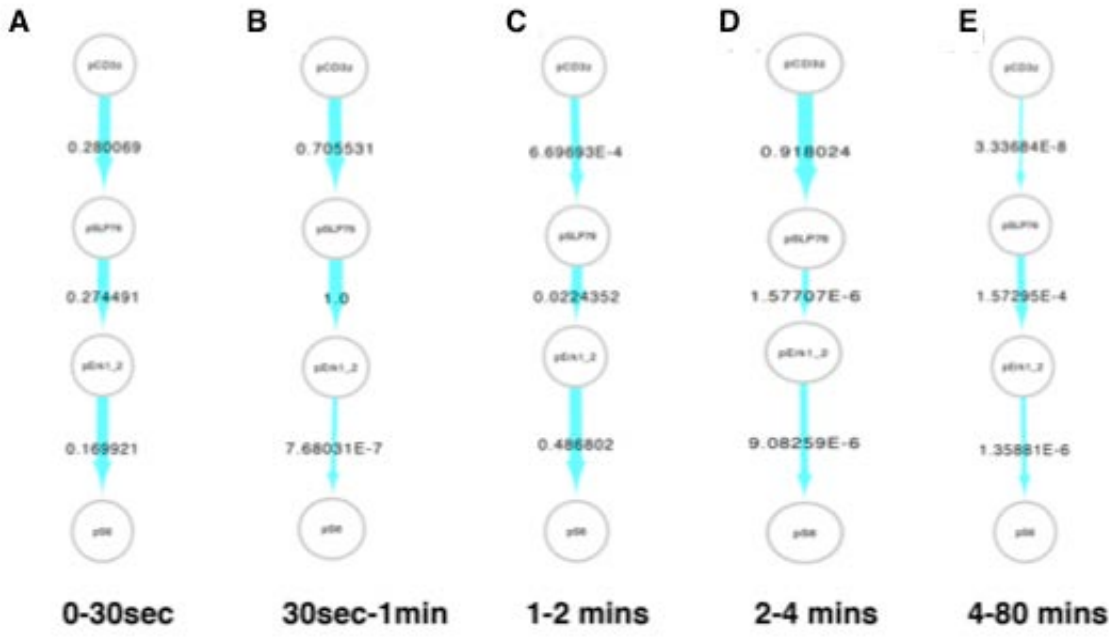

Fig. S6. In silico characterization of naïve CD4$^+$ T cell signaling stimulated with cross-linking antibodies against CD3, CD28, and CD4. (**A** to **E**) We used mass cytometry data derived from naïve CD4$^+$ T cells stimulated by CD3, CD28, and CD4 antibody crosslinking, which are available in the supplementary information of a study by Krishnaswamy *et al*. (*21*). We applied our data-driven framework (Fig. 3 and see Materials and Methods) to infer reaction fluxes in the pCD3ζ–pSLP-76–pERK–pS6 cascade following TCR activation. The fluxes are shown as cyan arrows with their values overlying the arrows. The thickness of an arrow is proportional to the value of the associated flux on a logarithmic scale. The reaction fluxes in this cascade corresponding to the cytometry data during the indicated time durations.

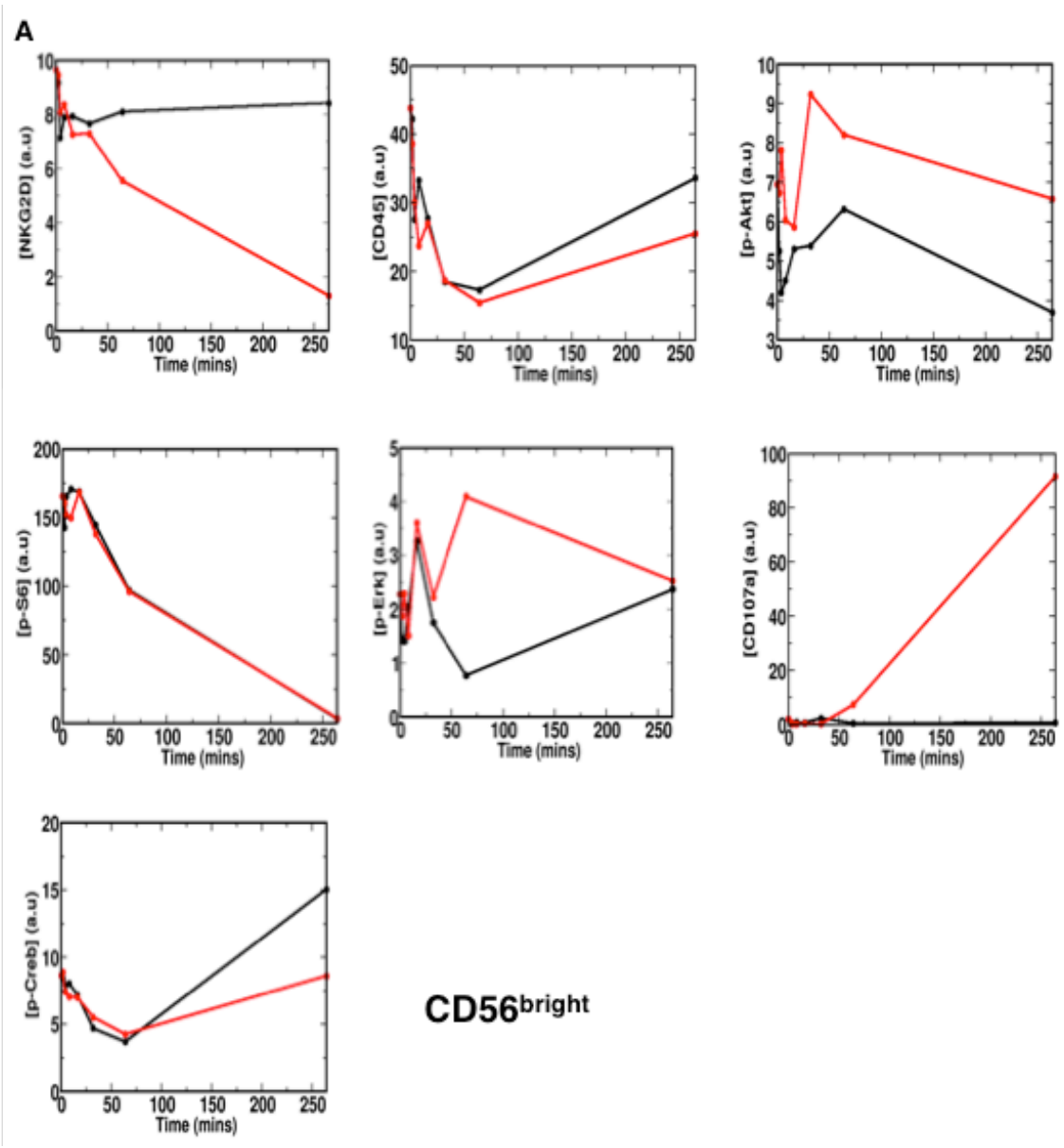
A
[NKG2D] (a.u)
[CD45] (a.u)
[p-Akt] (a.u)
[p-S6] (a.u)
[p-ErK] (a.u)
[CD107a] (a.u)
[p-Creb] (a.u)
Time (mins)
CD56bright

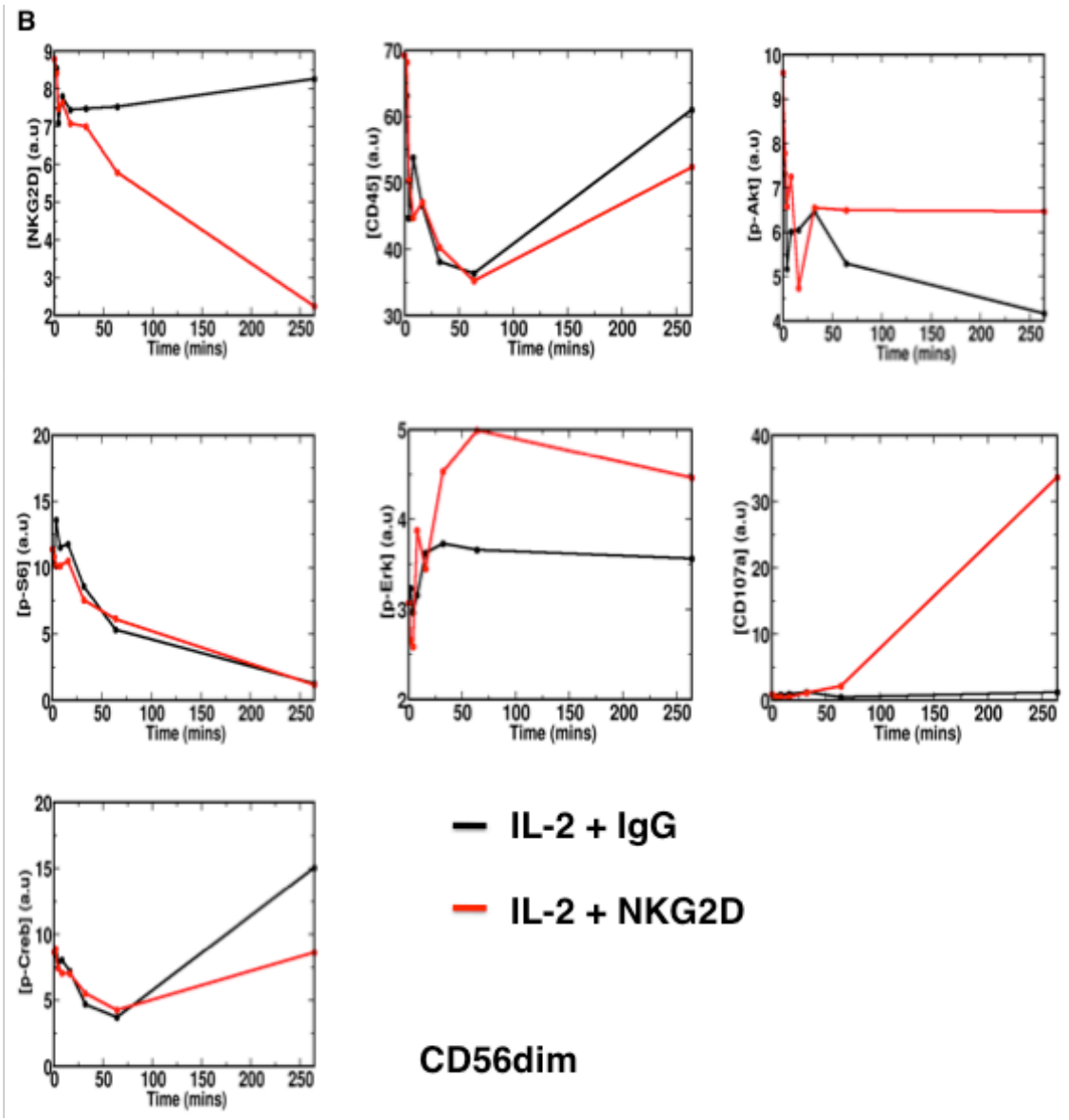

Fig. S7. Kinetics of the average abundances of proteins when IL-2-pretreated cells obtained from donor #3 were stimulated by either isotype-matched IgG or anti-NKG2D. (**A** and **B**) IL-2–treated CD56^{bright} (A) and CD56^{dim} (B) NK cells were pretreated with IL-2 for 24 hours and subsequently stimulated with anti-NKG2D mAb (red) or isotope-matched control Ab (black). Data are shown at the unstimulated condition (t = 0 min) and at multiple time points (t = 2, 4, 8, 16, 32, 64, and 264 min) after stimulation with control IgG (black) or anti-NKG2D mAb (red). The average protein abundances at each time point were calculated from Equation 3a, where N is the total number of cells. N = 3000 for CD56^{bright} NK cells stimulated with control IgG, N = 2500 for CD56^{bright} NK cells stimulated with anti-NKG2D, N = 25,500 for CD56^{dim} NK cells stimulated with control IgG, and N = 21,500 for CD56^{dim} NK cells stimulated with anti-NKG2D mAb.

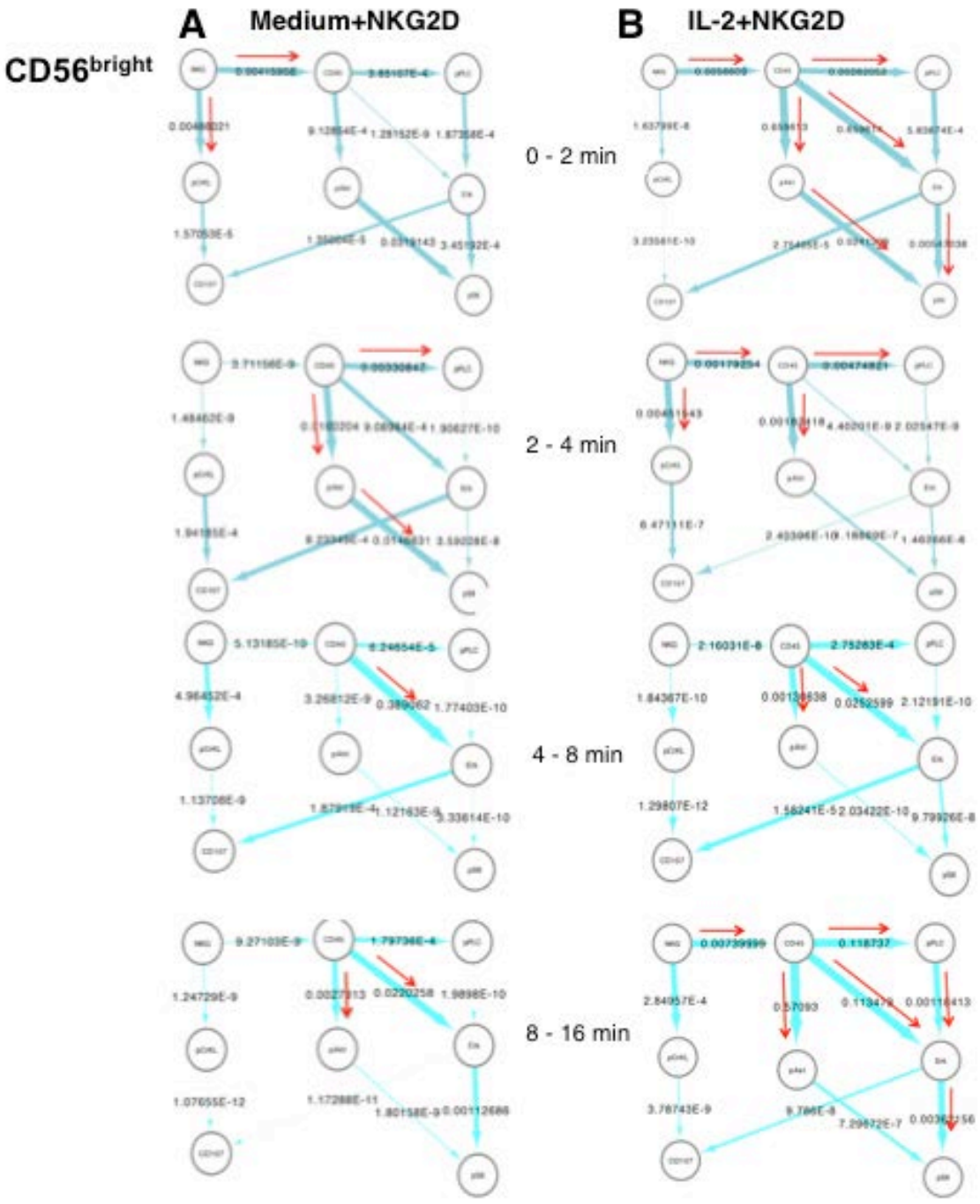
CD56bright
A
Medium+NKG2D
B
IL-2+NKG2D
0 - 2 min
2 - 4 min
4 - 8 min
8 - 16 min


2.10691E-8
2.47535E-5
0.0222506
7.93822E-4
3.87777E-9
0.00313636
2.00655E-11
5.1427E-10
7.48782E-10
0.00243817

16 - 32 min

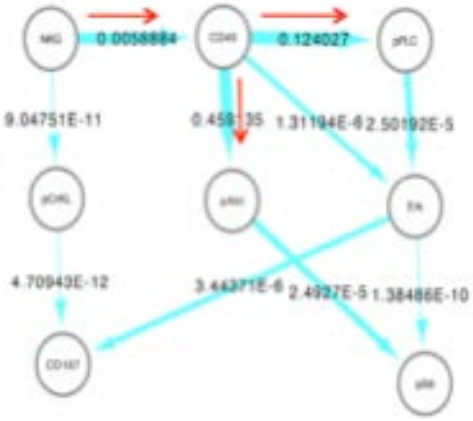
0.0058884
0.124027
9.04751E-11
0.459135
1.31194E-6
2.50192E-5
4.70943E-12
3.44371E-6
2.4927E-5
1.38486E-10

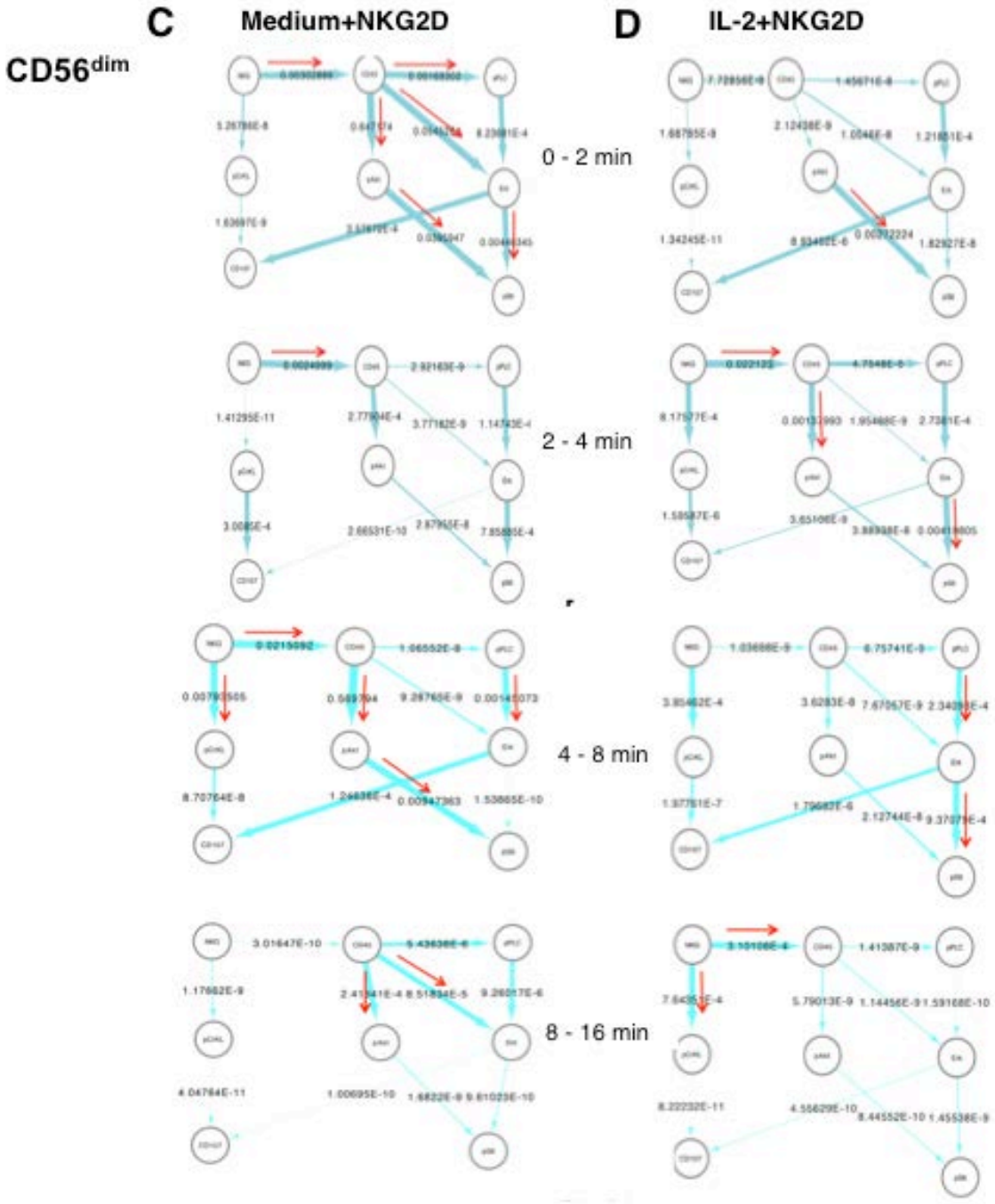
C
Medium+NKG2D
D
IL-2+NKG2D
CD56dim
0 - 2 min
2 - 4 min
4 - 8 min
8 - 16 min

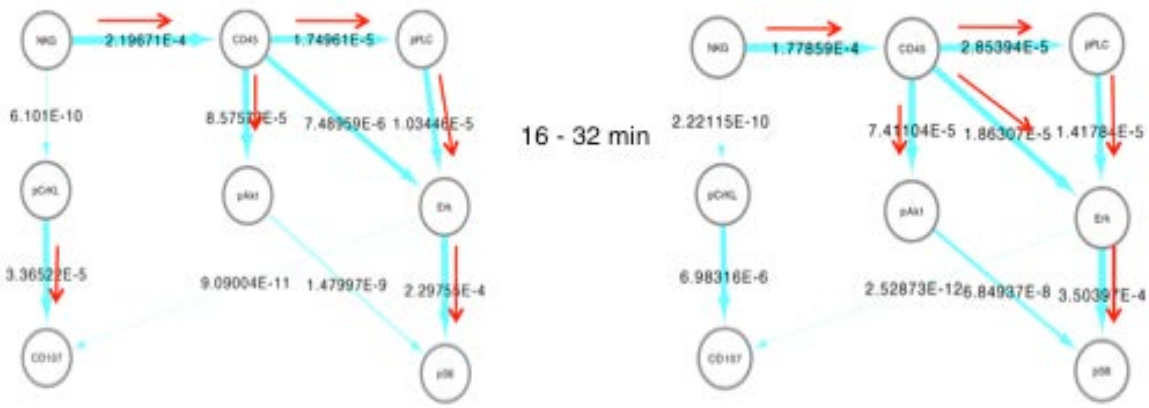

Fig. S8. In silico characterization of the NKG2D signaling kinetics in CD56^{bright} and CD56^{dim} NK cells from donor #2. (**A** and **B**) CD56^{bright} NK cells. The instantaneous fluxes are shown for the network presented in Fig. 4A. The fluxes were calculated using the mass cytometry data at two successive time points (as indicated) for CD56^{bright} NK cells pretreated with medium (A) or IL-2 (B) after stimulation with anti-NKG2D mAb). (**C** and **D**) CD56^{dim} NK cells. Fluxes, calculated for the same time intervals as those in (A and B), are shown for the medium-treated (C) or IL-2–treated (D) CD56^{dim} NK cells. Arrow thickness is proportional to the value (as indicated over arrows) of the associated flux on a logarithmic scale. The directions associated with relatively larger values of the fluxes are emphasized with red arrows. NKG and pPLC are used to denote NKG2D and, pPLC-γ2, respectively. The sample size (N) used for the four conditions are as follows: N = 672 for IL-2-treated CD56^{bright} NK cells, N = 1000 for medium-treated CD56^{bright} NK cells, N = 5300 for IL-2-treated CD56^{dim} NK cells, and N = 10,350 for medium-treated CD56^{dim} NK cells.

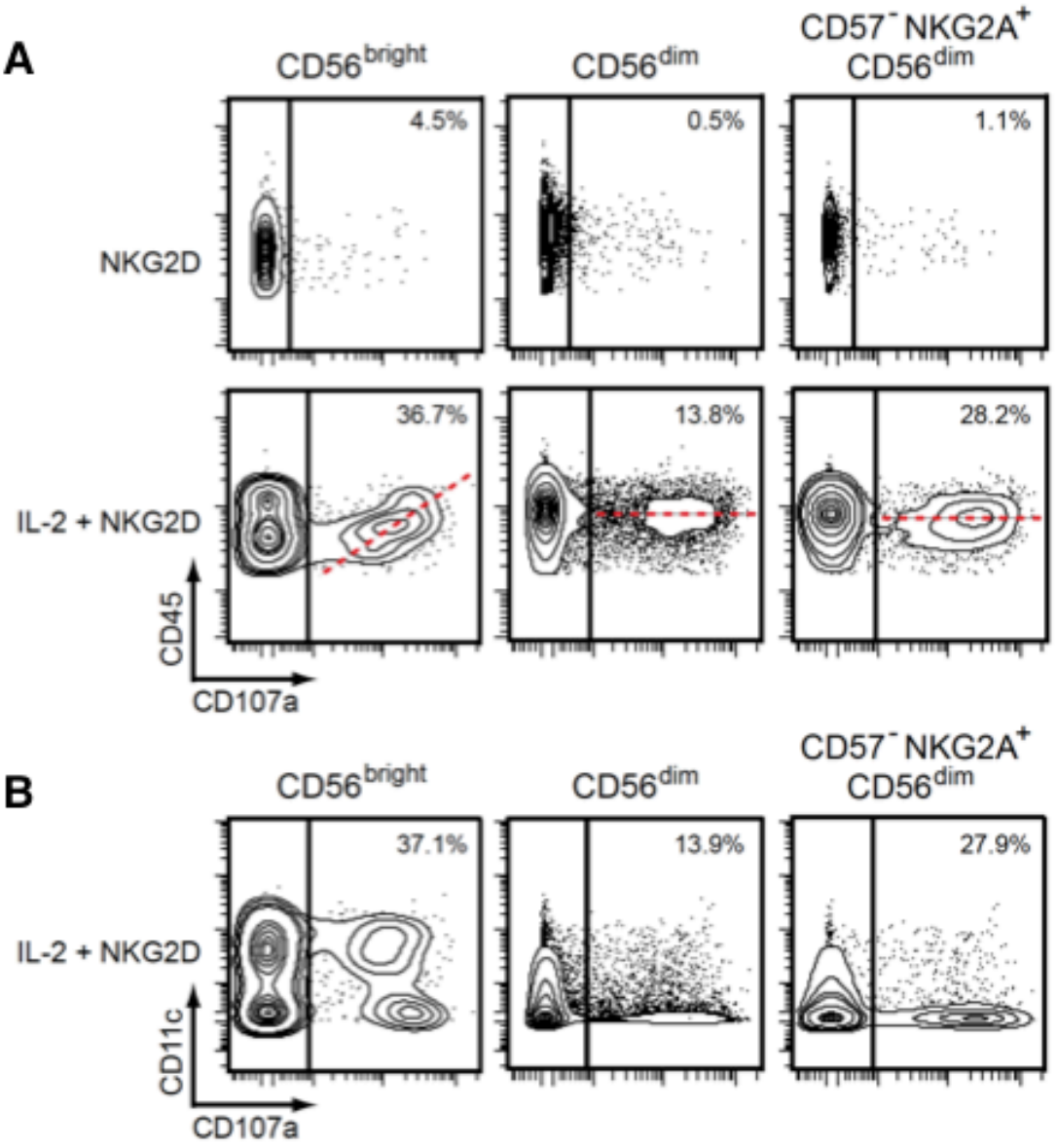

Fig. S9. Test of correlation between CD45 expression and CD107a mobilization to the cell surface of human NK cells from donor #2. (**A**) Mass cytometry analysis of CD45 and CD107a abundances 256 min after the stimulation of NKG2D on medium-treated and IL-2–treated $CD56^{bright}$, $CD56^{dim}$, and $CD57^{-}NKG2A^{+}CD56^{dim}$ NK cells. The dashed red line in each plot illustrates the correlation between the abundances of CD45 and CD107a. Numbers in the plots indicate the percentages of CD107a-positive cells. Data are from a single donor and are representative of five independent donors. (**B**) Mass cytometry analysis of CD11c and CD107a abundances 256 min after the stimulation of NKG2D on IL-2–treated $CD56^{bright}$, $CD56^{dim}$, and $CD57^{-}NKG2A^{+}CD56^{dim}$ NK cells. Numbers in the plots indicate the percentages of CD107a-positive cells. Data are from a single donor and are representative of five independent donors.

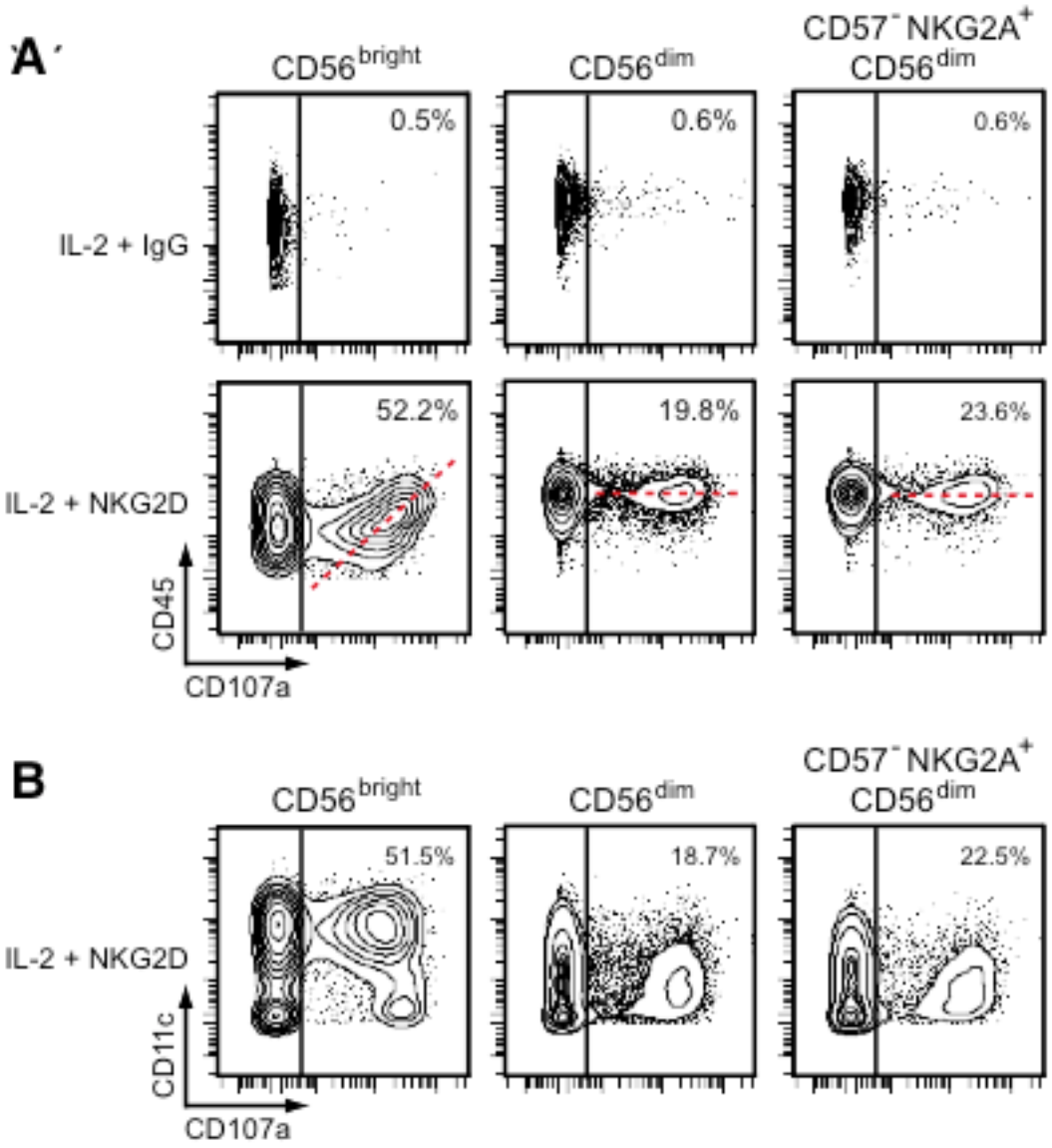

Fig. S10. Test of correlation between CD45 expression and CD107a mobilization to the cell surface of human NK cells from donor #3. (**A**) Mass cytometry analysis of CD45 and CD107a abundances 256 min after the incubation of IL-2–treated CD56^{bright} and CD56^{dim} NK cells with isotype-matched Ig control antibody (IgG) or anti-NKG2D mAb. The dashed red line in each plot illustrates the correlation between the abundances of CD45 and CD107a. Numbers in the plots indicate the percentages of CD107a-positive cells. Data are from a single donor and are representative of five independent donors. (**B**) Mass cytometry analysis of CD11c and CD107a abundances 256 min after the stimulation of IL-2–treated CD56^{bright} and CD56^{dim} NK cells with anti-NKG2D mAb. Numbers in the plots indicate the percentages of CD107a-positive cells. Data are from a single donor and are representative of five independent donors.

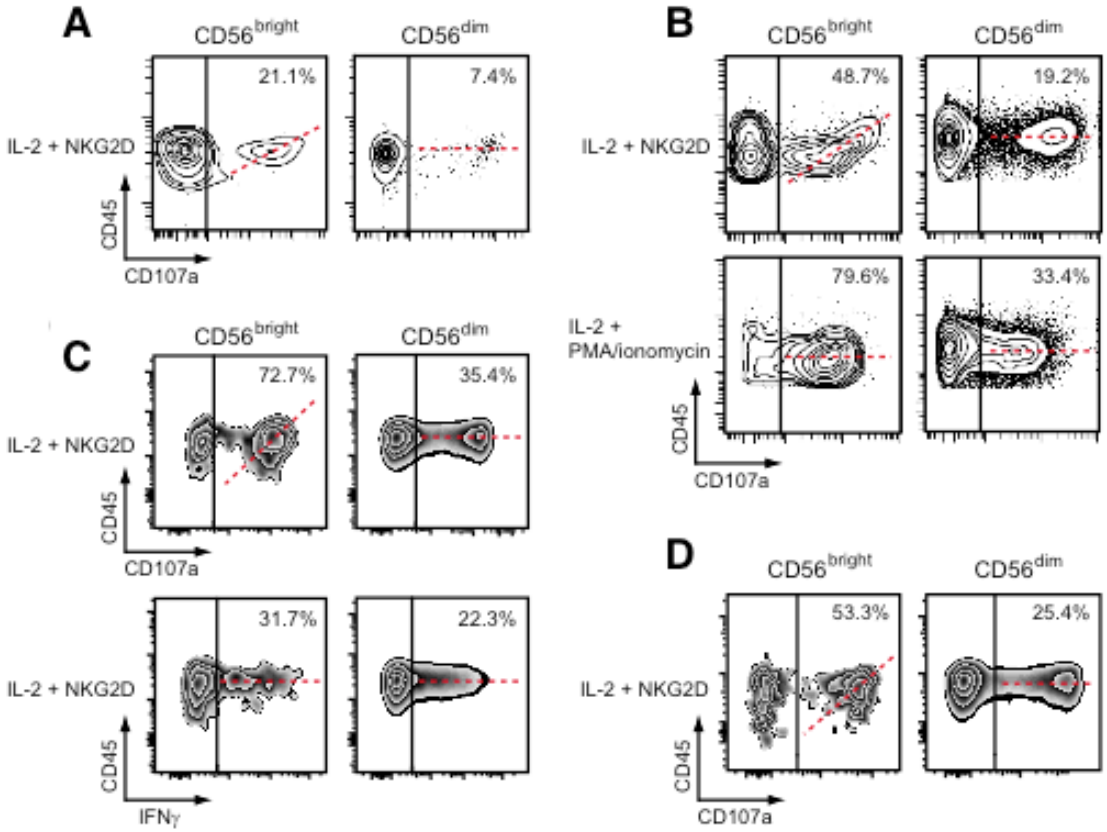

Fig. S11. Test of correlation between CD45 expression and CD107a mobilization to the cell surface of human NK cells from donors #4 to #7. (**A**) Mass cytometry analysis of CD45 and CD107a abundances 256 min after the stimulation of IL-2–treated CD56^{bright} and CD56^{dim} NK cells from donor #4 with anti-NKG2D mAb. Data are from a single donor and are representative of five independent donors. (**B**) Top: Mass cytometry analysis of CD45 and CD107a abundances 256 min after the stimulation of IL-2–treated CD56^{bright} and CD56^{dim} NK cells from donor #5 with anti-NKG2D mAb. Bottom: Mass cytometry analysis of CD45 and CD107a abundances 256 min after the stimulation of IL-2–treated CD56^{bright} and CD56^{dim} NK cells from donor #5 with PMA and ionomycin. Data are from a single donor and are representative of three independent donors. (**C**) Top: Flow cytometry analysis of CD45 and CD107a abundances 256 min after the stimulation of IL-2–treated CD56^{bright} and CD56^{dim} NK cells from donor #6 with anti-NKG2D mAb. Bottom: Flow cytometry analysis of CD45 and IFN-γ abundances 256 min after the stimulation of IL-2–treated CD56^{bright} and CD56^{dim} NK cells from donor #6 with anti-NKG2D mAb. Data are from a single donor and are representative of two independent donors. (**D**) Flow cytometry analysis of CD45 and CD107a abundances 256 min after the stimulation of IL-2–treated CD56^{bright} and CD56^{dim} NK cells from donor #7 with anti-NKG2D mAb. Data are from a single donor and are representative of two independent donors.The dashed red line in each plot illustrates the correlation between the abundances of CD45 and either CD107a or IFN-γ. Numbers in the plots indicate the percentages of CD107a- or IFN-γ-positive cells.

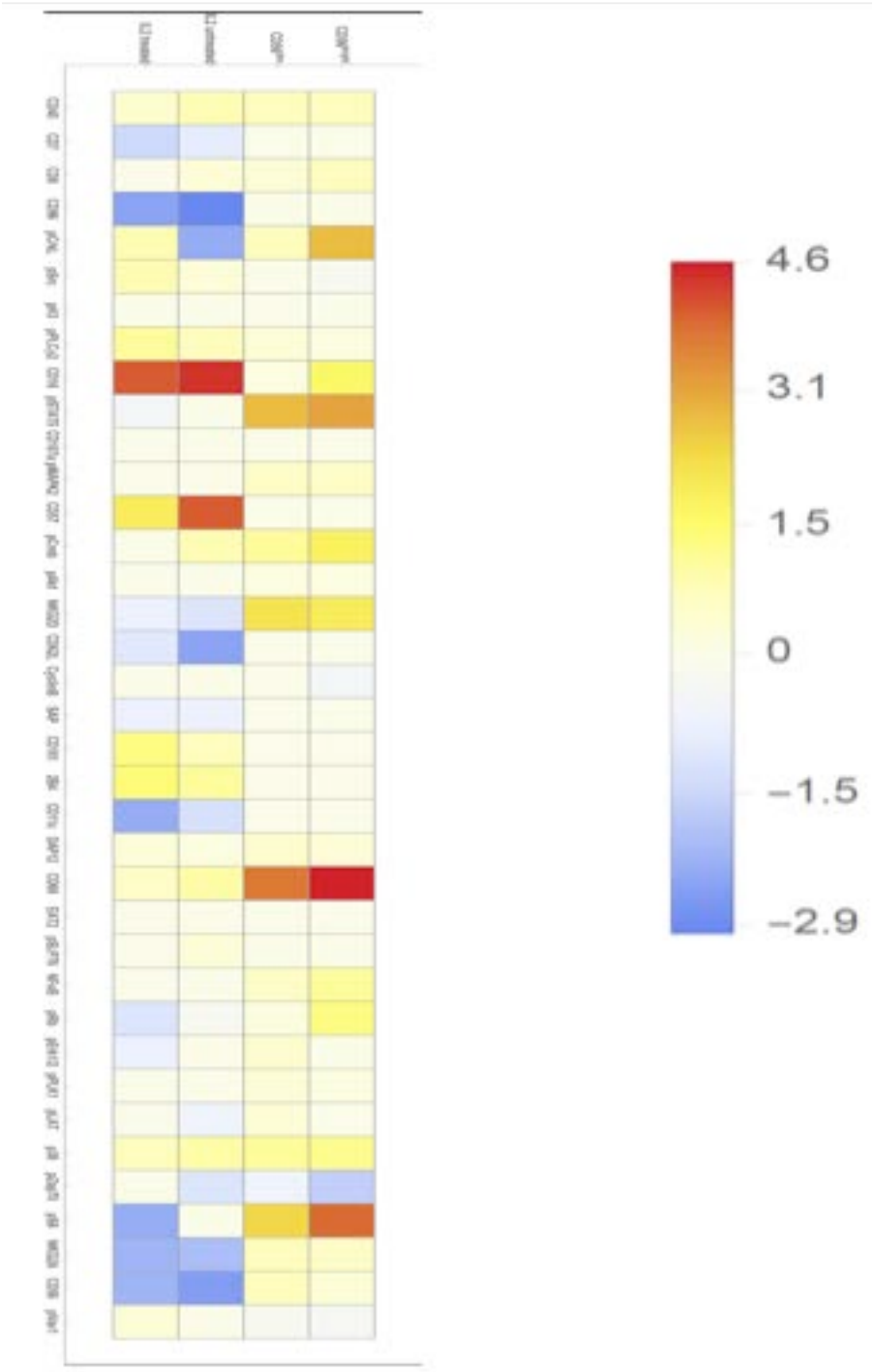

Fig. S12. Matrix plot showing the changes in average protein abundances in CD56^{bright} and CD56^{dim} NK cells in response to IL-2. The fold-changes in average protein abundances between IL-2 treatment and medium treatment in CD56^{bright} and CD56^{dim} NK cells are shown using a color plot. Right: The gradient bar indicates the extent of the fold-change.

Table S1. Changes in average protein abundances in CD56^{bright} and CD56^{dim} NK cells in response to IL-2. The data are derived from experiments with human NK cells isolated from donor #1. Data are from a single donor and are representative of two independent donors. The names of the proteins considered in our model (Fig. 4A) are shown in bold. The cases for large changes (increase or decrease) are shown in blue or orange boxes for better visualization.

Protein	**Changes upon IL-2 incubation (from untreated to treated) in the CD56 subsets**		**Differences with CD56 expression (from bright to dim) within the same IL-2 condition**	
	CD56^{bright}	**CD56^{dim}**	**IL-2-untreated**	**IL-2-treated**
CD45	increase (>1.5-fold)	increase (>1.5-fold)	increase (>1.6-fold)	increase (>1.3-fold)
CD7	not substantial	not substantial	decrease(>1.8-fold)	large decrease(>2.8-fold)
CD8	increase (>1.5-fold)	increase (>1.2-fold)	small increase (>1.2-fold)	no appreciable change
CD96	not substantial	not substantial	large decrease (>17-fold)	large decrease (>9 fold)
pCrkL	Decrease (~6-fold)	Small increase (>1.5-fold)	large decrease (>8-fold)	increase (>1.6-fold)
pSrc	not substantial decrease (>1.1-fold)	not substantial decrease (>1.01-fold)	small increase (>1.2-fold)	increase (>1.6-fold)
pH3	not substantial	not substantial	not substantial	not substantial
pPLC γ 2	not substantial increase (>1.1-fold)	not substantial increase >1.2-fold)	increase (>1.5-fold)	increase (>1.8-fold)
CD16	increase (>2.5-fold)	small increase (>1.1-fold)	substantial increase (>90-fold)	substantial increase (>50-fold)
pSTAT5	large increase (>15-fold)	large increase(>9-fold)	not substantial	small decrease (>1.3-fold)
CD107a	very little change,	very little change,	very little change,	very little change,

	however, it increases substantially post-NKG2D stimulation in the IL-2-treated cells	however, it increases substantially post-NKG2D stimulation in the IL-2-treated cells	however, it increases post-NKG2D stimulation in the bright cells	however, it increases post-NKG2D stimulation in the bright cells
pMAPKAPK2	small increase (>1.4-fold)	small increase (>1.4-fold)	not substantial, increases in both cell types post-NKG2D stimulation	not substantial, increases in both cell types post-NKG2D stimulation
CD57	Increase, but not substantial	Increase	substantial increase (>50-fold)	large increase (>3-fold)
pCreb	large increase (>2.9-fold)	increase(>1.8-fold)	increase (>1.6-fold)	not substantial
pAkt	not substantial increase (>1.1-fold)	not substantial increase (>1.1-fold)	not substantial	not substantial
NKG2D	large increase (>3-fold)	large increase (>3.8-fold)	decrease (>2-fold)	decrease (>1.6-fold)
CD62L	Decrease	Not substantial	large decrease (>9-fold)	decrease (>1.9-fold)
cyclin B	no substantial decrease (>1.3 fold)	no substantial change	no substantial change	no substantial change
SAP	no substantial change	no substantial change	decrease (>1.6-fold)	decrease (>1.6-fold)
CD161	Not substantial	Increase	increase (>1.5-fold)	increase (>2-fold)
2B4	Slight increase	Increase	increase (>1.8-fold)	increase (>2.1-fold)
CD11c	Increase	Increase	decrease (>2.2 fold)	large decrease (>8 fold)
DAP12	small increase (>1.2-fold)	small increase (>1.3-fold)	small increase (>1.1-tfold)	small increase (>1.2-fold)
CD69	large increase (>100-fold)	large increase (>40-fold)	small increase (>1.7-fold)	small decrease (>1.4-fold)

EAT2	no substantial change	no substantial change	no substantial change	no substantial change
pSLP76	no substantial change	no substantial change	small increase (>1.2-fold)	hardly any increase (>1.09-fold)
NFkB	increase (>1.8-fold)	increase (>1.4-fold)	no substantial change	no substantial change
pRb	increase (>2-fold)	small increase (>1.1-fold)	small decrease (>1.1-fold)	decrease (>2-fold)
pErk-1/2	increase (>2-fold). pErk increases in the IL-2-treated cells post-NKG2D stimulation.	small increase (>1.3-fold). pErk increases in the IL-2-treated cells post-NKG2D stimulation.	no substantial change	decrease (>1.6-fold)
pPlk1	small increase (>1.1-fold), increases in the IL-2-treated cells post-NKG2D stimulation.	small increase (>1.2-fold), increases in the IL-2-treated cells post-NKG2D stimulation.	no substantial change	no substantial change
pLAT	no substantial change	small increase (>1.2 fold)	decrease (>1.5-fold)	hardly any decrease (>1.1-fold)
p38	increase (>1.9-fold)	increase (>1.8-fold)	increase (>1.7-fold)	increase (>1.5-fold)
pZAP70	large decrease (>3.5-fold)	decrease (>1.5-fold)	decrease (>2-fold)	no substantial change, however, increases almost 2 times in the bright cells post-NKG2D stimulation
pS6	very large increase (>46-fold)	large increase (>5-fold)	hardly any decrease (>1.09-fold)	large decrease (>8-fold)

NKG2A	increase (>1.4-fold)	increase (>1.5-fold)	large decrease (>6-fold)	large decrease (>7-fold)
CD56	increase (>1.2-fold)	increase (>1.5-fold)	large decrease (>10-fold)	large decrease (>7-fold)
pVav1	small decrease (>1.2-fold)	small decrease (>1.1-fold)	not substantial	small increase (>1.2-fold)

Table S2. Mass cytometry antibody panel.
Antibodies purchased from Fluidigm were conjugated to the indicated metal by the manufacturer. All other antibodies were conjugated to the indicated metal with the MaxPAR antibody-conjugation kit (Fluidigm) according to the manufacturer's recommended protocol. Successful conjugation was subsequently verified and all of the antibodies were titrated before use.

	Marker	**Metal**	**Antibody Clone**	**Vendor**
Surface	CD45	113In	HI30	BioLegend
	CD7	115In	CD7-6B7	BioLegend
	CD8	139La	RTA-T8	BioLegend
	CD3+CD235+CD61	141Pr	UCHT1+HIR2+VI-PL2	BioLegend
	CD96	142Nd	NK92.39	BioLegend
	CD57	147Sm	HCD57	BioLegend
	CD16	148Nd	3G8	Fluidigm
	CD107a	151Eu	H4A3	Fluidigm
	NKG2D	154Sm	1D11	BioLegend
	CD62L	155Gd	DREG-56	BioLegend
	CD161	158Gd	191B8	Beckman Coulter
	CD11c	159Tb	Bu15	Fluidigm
	2B4	160Gb	PP35	eBioscience
	CD69	162Dy	FN50	Fluidigm
	NKG2A	174Yb	Z199	Beckman Coulter
	CD56	176Yb	NCAM16.2	BD
Surface/ Intracellular	CD33+CD20+cPARP+cCaspase 3	173Yb	WM53+H1+ F21-852+C92-605	BioLegend BD
Intracellular	pCrkL(Y207)	143Nd	Polyclonal	Fluidigm
	pSrc(Y418)	144Nd	K98-37	BD
	histone H3(S28)	145Nd	HTA28	BioLegend
	pPLC γ 2(Y759)	146Nd	K86-689.37	BD
	pCreb(S133)	149Sm	87G3	Cell Signaling
	pSTAT5(Y694)	150Nd	47	BD
	pAkt(S473)	152Sm	D9E	Fluidigm
	pMAPKAPK2(T334)	153Eu	27B7	Cell Signaling
	Cyclin B	156Gd	GNS-1	BD
	SAP	157Gd	XLP-1D12	Cell Signaling
	DAP12	161Dy	406288	R&D Systems
	EAT2	163Dy	Polyclonal	Abgent

	pSLP76(Y128)	164Dy	J141-668.36.58	BD
	pNF κ B(S529)	165Ho	K10-895.12.50	BD
	pRb(S807/S811)	166Er	J112-906	BD
	pErk1/2(T202/Y204)	167Er	D13-14-4E	Fluidigm
	pPlk1(T210)	168Er	K50-483	BD
	pP38(T180/Y182)	169Tm	36/p38	BD
	pLAT(Y226)	170Er	J96-1238.58.93	BD
	pZAP70(Y319/Y352)	171Yb	17a	Fluidigm
	pS6(S235/S236)	172Yb	N7-548	Fluidigm
	pVav1(Y160)	175Lu	Polyclonal	Life Technology